



**HAL**  
open science

## The high-accuracy spectroscopy of H<sub>2</sub> rovibrational transitions in the (2-0) band near 1.2 $\mu\text{m}$

H. Fleurbaey, A. Koroleva, S. Kassi, A. Campargue

► **To cite this version:**

H. Fleurbaey, A. Koroleva, S. Kassi, A. Campargue. The high-accuracy spectroscopy of H<sub>2</sub> rovibrational transitions in the (2-0) band near 1.2  $\mu\text{m}$ . *Physical Chemistry Chemical Physics*, 2023, 25 (21), pp.14749-14756. 10.1039/d3cp01136d . hal-04221906

**HAL Id: hal-04221906**

**<https://hal.science/hal-04221906v1>**

Submitted on 14 Nov 2023

**HAL** is a multi-disciplinary open access archive for the deposit and dissemination of scientific research documents, whether they are published or not. The documents may come from teaching and research institutions in France or abroad, or from public or private research centers.

L'archive ouverte pluridisciplinaire **HAL**, est destinée au dépôt et à la diffusion de documents scientifiques de niveau recherche, publiés ou non, émanant des établissements d'enseignement et de recherche français ou étrangers, des laboratoires publics ou privés.

1 High accuracy spectroscopy of H<sub>2</sub> rovibrational transitions  
2 in the (2-0) band near 1.2 μm

3  
4 H. Fleurbaey<sup>1</sup>, A.O. Koroleva<sup>1,2</sup>, S. Kassi<sup>1</sup>, A. Campargue<sup>1,\*</sup>  
5  
6

7  
8 <sup>1</sup> Univ. Grenoble Alpes, CNRS, LIPhy, Grenoble, France  
9 <sup>2</sup> Institute of Applied Physics of RAS, Nizhniy Novgorod, Russia  
10  
11  
12

13 Accurate transition frequencies of six lines of the (2-0) vibrational band of H<sub>2</sub> are measured near  
14 1.2 μm, namely Q1-Q4, S0 and S1. These weak electric-quadrupole transitions were measured at room  
15 temperature by comb referenced cavity ring-down spectroscopy. Accurate transition frequencies were  
16 determined applying a multi-spectrum fit procedure with various profile models including speed  
17 dependent collisional broadening and shifting phenomena. Although none of the considered profiles  
18 allows reproducing the shape of the strongest lines at the noise level, the zero-pressure line centers are  
19 found mostly independent on the used profile. These values are the first H<sub>2</sub> (2-0) transition frequencies  
20 referenced to an absolute frequency standard. As a result, a 1σ-accuracy better than 100 kHz is  
21 achieved for the Q1, S0 and S1 transition frequencies, improving by three orders of magnitude the  
22 accuracy of previous measurements. For the six measured transitions, the most recent calculated  
23 frequencies are found systematically underestimated by about 2.58 MHz, about twice their claimed  
24 uncertainties. The energy separation between the  $J=2$  and  $J=0$  rotational levels of the vibrational  
25 ground state is derived from the Q2 and S0 transition frequencies and found within the 110 kHz  
26 uncertainty of its theoretical value. The same level of agreement is achieved for the energy separation  
27 between the  $J=3$  and  $J=1$  rotational levels obtained by difference of the Q3 and S1 transition  
28 frequencies. The *ab initio* values of the intensity of the six transitions are validated within a few  
29 thousandths.

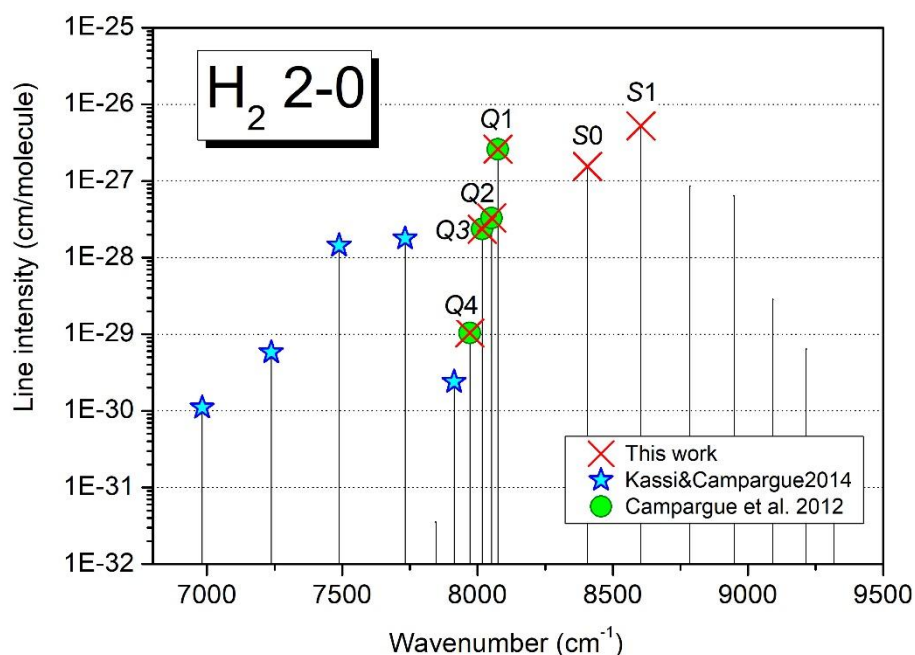
30  
31 \* Corresponding author: E-mail: [alain.campargue@univ-grenoble-alpes.fr](mailto:alain.campargue@univ-grenoble-alpes.fr)  
32

## 33 Introduction

34 Due to its simplicity, dihydrogen ( $H_2$ ) and its isotopologues (HD and  $D_2$ ) are quantum physics  
35 test systems for advanced theoretical calculations including nonadiabatic, relativistic, quantum  
36 electrodynamics (QED) effects [1], [2], [3], and hyperfine structure calculations [4], [5], [6]. For  
37 instance, the measurement of highly accurate rotation-vibration (RV) transition frequencies provide  
38 stringent tests of the level energies recently obtained by fully variational calculations including high  
39 level QED corrections [1], [2], [3]. In recent years, significant progress has resulted from the fruitful  
40 emulation between theory and experiment. Due to the weakness of the considered RV transitions,  
41 precision spectroscopy is experimentally challenging in  $H_2$ . As a homonuclear diatomic molecule,  $H_2$   
42 has no electric dipole spectrum and its RV spectrum is formed by very weak electric-quadrupole  
43 vibrational bands, (V-0), of decreasing intensity (see Fig. 6 of Ref. [7]). For instance, the (1-0)  
44 fundamental and (2-0) first overtone bands centered at about 4160 and 8090  $cm^{-1}$ , have maximum line  
45 intensity of  $3.2 \times 10^{-26}$  and  $5.2 \times 10^{-27}$  cm/molecule at 296 K, respectively. In the recent years, hydrogen  
46 deuteride (HD) has been preferred for metrological measurements because HD shows stronger  
47 absorption bands than  $H_2$ . This is due to the charge asymmetry and resulting weak dipole moment  
48 existing in this heteronuclear isotopologue giving rise to a small electric dipole moment. As a result, in  
49 the (2-0) band, the electric dipole transitions in HD are about two orders of magnitude stronger than  
50 electric quadrupole transitions in  $H_2$  (and HD).

51 Accuracies better than 100 kHz level have been recently achieved by several groups for a few  
52 (2-0) transition frequencies in HD [8], [9], [10], [11], [12], [13], [14], [15], [16], [17]. This level of  
53 accuracy represents about one thousandth of the Doppler width of the (2-0) HD transitions at room  
54 temperature. Part of the experimental studies were performed in saturation regime in order to  
55 circumvent this large Doppler broadening but underlying hyperfine components were found to lead to  
56 dispersive-like spectral structure which limited the final accuracy on the line center determination [8],  
57 [10], [11], [12], [14]. As a result, accuracies on HD transition frequencies achieved in saturation  
58 regime are similar to those obtained in Doppler regime [15], [16], in particular at low temperature  
59 [17].

60 To the best of our knowledge, in the case of the  $H_2$  major isotopologue, no RV transition  
61 frequencies have been reported with sub-MHz accuracy, so far. This matter of fact results both from  
62 the above-mentioned weakness of the  $H_2$  RV transitions and from the lack of recent measurements of  
63  $H_2$  spectra referenced to frequency standards. In this context, let us mention the S3 electric-quadrupole  
64 transition of the (3-0) band near 795 nm reported with a 1.6 MHz accuracy by measuring the  
65 frequency shift to a Rb line [18], [19]. Regarding the (2-0) band presented in **Fig. 1**, the most accurate  
66 measurements were performed in our group by high sensitivity cavity ring down spectroscopy (CRDS)  
67 but the frequency calibration of these spectra were based on nearby reference lines of water vapor  
68 (present as an impurity in the  $H_2$  cell) [7], [20]. As a result, the claimed uncertainty on the reported  
69 transition frequencies was no better than  $10^{-3} cm^{-1}$  (30 MHz).



70

71 **Figure 1.** Calculated stick spectrum of the (2-0) band of  $H_2$  [21]. Absorption lines previously measured by  
 72 CRDS [7], [20] are highlighted. The rotational labeling is indicated for the six transitions presently measured.

73 In the present work, we report a gain of up to three orders of magnitude on high accuracy  
 74 frequency measurements of the Q1-Q4 transitions and complement the dataset with S0 and S1, in the  
 75 (2-0) vibrational band of  $H_2$ . The measurements were performed in Doppler regime at room  
 76 temperature, by comb referenced cavity ring-down spectroscopy. As just mentioned, the Q1-Q4  
 77 transitions have been measured in [20] using standard CRDS while the S0 and S1 transitions were  
 78 apparently not revisited since the recordings of Bragg et al. in 1982 [22]. These authors used the Kitt  
 79 Peak Solar Fourier transform spectrometer with an absorption pathlength of 434 m and pressure values  
 80 of 1.4 and 2.8 atm.

81 Let us recall that the determination of the transition frequencies in Doppler regime requires to  
 82 correct the pressure-induced line shift in order to extrapolate the line center at zero pressure limit. This  
 83 necessitates for a careful line profile analysis of series of recordings at different pressures to determine  
 84 the pressure dependence of each spectroscopic parameter. As non-Voigt line-shape effects (*e.g.* Dicke  
 85 narrowing and speed-dependent effects) are exceptionally pronounced in the case of  $H_2$  (see [23] and  
 86 [24]), sophisticated line shapes such as the speed-dependent Nelkin-Ghatak profile will be used in the  
 87 forthcoming analysis. Note that the high sensitivity provided by cavity-enhanced techniques like  
 88 CRDS is a crucial advantage as high quality recordings at low pressure (*e.g.* a few Torr in the present  
 89 case of the Q1, S0 and S1 lines) limit the uncertainty on the line center extrapolation at zero-pressure.

90 The experimental setup and the recording procedure are described in the following section. In  
 91 the next one, we present the frequency determination of the different transitions from a multi-spectrum

92 fit of the series of spectra recorded at different pressures. The obtained transition frequencies are  
93 compared with theory in the penultimate section, before the concluding remarks.

### Experiment

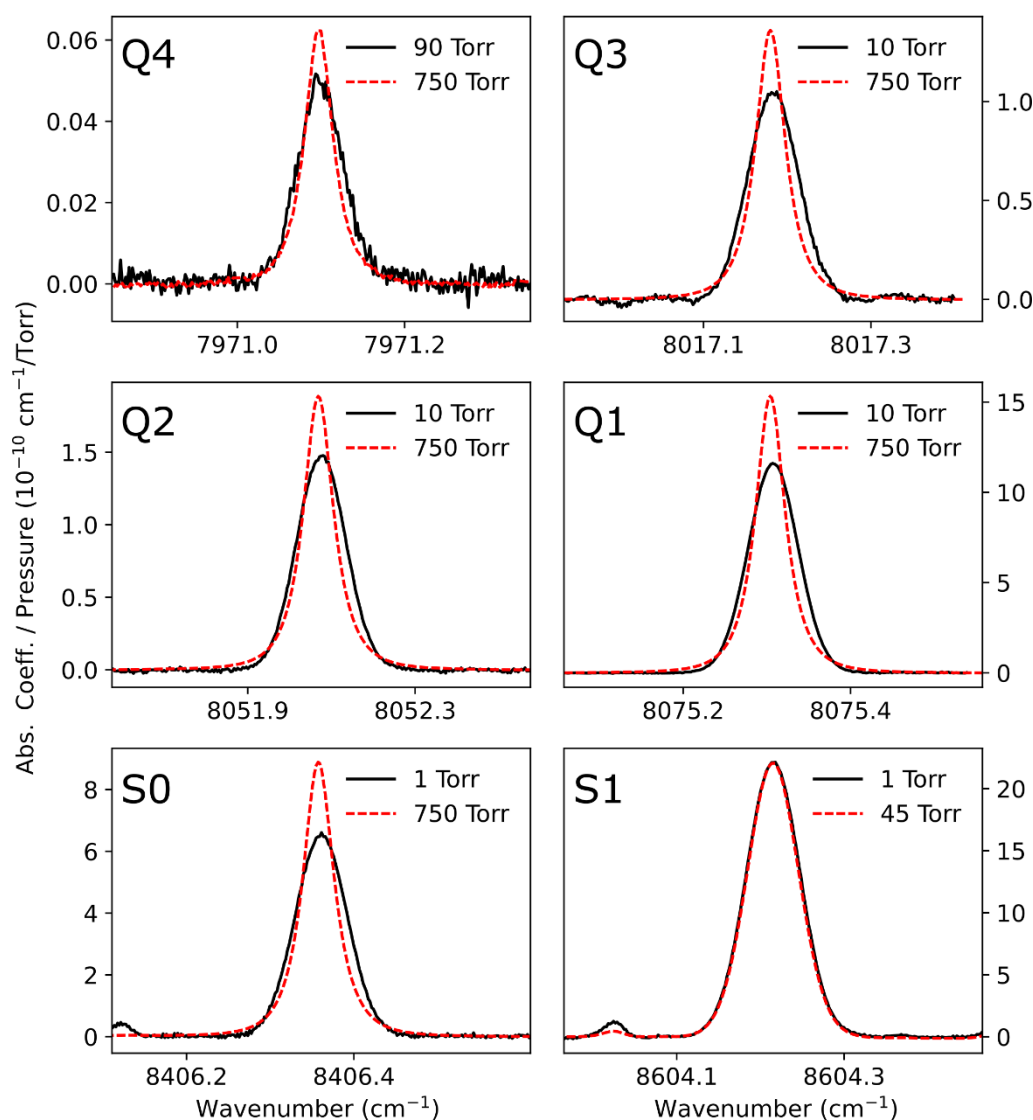
94 The room temperature absorption spectrum of natural dihydrogen (Alphagaz2, 99.9999 %  
95 chemical purity) was recorded in flow regime by high sensitivity frequency comb referenced cavity  
96 ring-down spectroscopy. The frequency CR-CRDS method and setup used for the recordings have  
97 been described in details in Refs. 25], [26]. The accurate frequency values associated “on the fly” to  
98 each ring-down event allow not only for an absolute calibration of the frequency axis but also for a  
99 reduction of the noise amplitude in particular on the sharp slopes of the line profiles [27], [28].

100 The recording procedure is similar to that adopted to measure D<sub>2</sub> transitions in the (2-0) band  
101 [26], [29], [30] except that an external cavity diode laser (ECDL) is used as light source instead of  
102 distributed-feedback (DFB) laser diodes. The ECDL (Toptica fiber-connected DL pro, 1200 nm) was  
103 tuned to record small spectral intervals around the Q1-Q4, S0 and S1 transitions spanning the 7970 -  
104 8605 cm<sup>-1</sup> region. For the evacuated cavity, the ring-down time  $\tau_0$  varied from about 180  $\mu$ s to 360  $\mu$ s  
105 depending on wavenumber. For each frequency point, about 50 to 120 ring-downs were averaged  
106 leading to a minimum detectable absorption coefficient between  $2 \times 10^{-12}$  and  $6 \times 10^{-11}$  cm<sup>-1</sup> for a single  
107 scan. Following [27], [29], a self-referenced frequency comb (Model FC 1500-250 WG from Menlo  
108 Systems) was used for the frequency calibration of the spectra. The frequency attached to each ring  
109 down event is determined from (i) the frequency measurement of the beat note between a fraction of  
110 the ECDL light and a tooth of the frequency comb and (ii) the tooth number deduced from the  
111 frequency value provided by a commercial Fizeau type wavemeter (HighFinesse WSU7-IR, 5 MHz  
112 resolution, 20 MHz accuracy over 10 hours). For each frequency step, the average central emission  
113 frequency of the ECDL was actively stabilized using a software based Proportional-Integral loop, with  
114 100 Hz bandpass, acting on the laser current.

115 A drawback of Doppler limited absorption spectroscopy compared to Doppler-free saturation  
116 spectroscopy is that the retrieved line parameters can be affected by interferences with lines due to gas  
117 impurities present in the cell. Water vapor desorbing from the CRDS cell or from the injection tubes is  
118 the most problematic species. In order to minimize the concentration of gas impurities, the spectra  
119 were recorded in flow regime. As explained in the next section, water lines were apparent in some of  
120 the spectra and allowed to estimate the water concentration in the cell to be typically a few tens of  
121 ppm.

122 The hydrogen pressure in the CRDS cell was actively regulated to values between 1.0 and 750  
123 Torr through a needle valve connecting the cell to a turbo pump group, using a computer based  
124 Proportional/Integral controller. The gas pressure in the cell was continuously monitored by two  
125 capacitance gauges (MKS Baratron, 10 Torr and 1000 mbar full range). For each line, the recordings  
126 were performed for a series of pressure values listed in **Table 1**. The range of the pressure values  
127 depends on the line intensities. In the case of the Q4 line which has the smallest intensity (about  $10^{-29}$

128 cm/molecule), a minimum pressure value of 90 Torr was used as the quality of the spectra was  
 129 insufficient at lower pressure. In the case of the strongest lines (Q1, S0 and S1) which have an  
 130 intensity larger than  $10^{-27}$  cm/molecule range, recordings could be performed down to 1 Torr. The  
 131 strong pressure impact on the line profiles is illustrated in **Fig. 2**. For each line, the absorption  
 132 coefficients obtained for the lowest and highest pressure values have been divided by the pressure  
 133 values (in Torr) and superimposed. The self-induced pressure shift of the line centre and the narrowing  
 134 of the profile at higher pressure are clearly observed. From the relative area of water lines visible in S0  
 135 and S1 spectra one concludes that water is essentially desorbed from the tubing and/or cell rather than  
 136 present in the sample bottle, as its relative amount clearly varies with pressure.



137  
 138 **Fig. 2** Comparison of the profile of the six (2-0)  $H_2$  lines observed in this work, for the lowest and highest  
 139 pressure value of each dataset. For the clarity of the figure, the absorption coefficients have been corrected from  
 140 the baseline and divided by the pressure values in Torr. Note the pressure shift of the line centre and the  
 141 narrowing of the profile at higher pressure.

142 In order to improve the line parameter determinations, for each pressure value, a number of  
 143 spectra were recorded successively (from 5 to 72 – see **Table 1**). The duration of a single scan was

144 about 20 minutes. Special efforts were made to accumulate spectra for the lowest pressure values  
 145 which are crucial to minimize the uncertainty on the zero-pressure line position. In the case of the Q1  
 146 line, in addition to the recordings listed in **Table 1**, series of 30 to 100 spectra were recorded between  
 147 2 and 10 Torr, with a pressure step of 1 Torr (525 spectra in total). Those spectra were analyzed as an  
 148 independent dataset because that measurement campaign was separated from the others by several  
 149 years. The temperature varied between 294.0 and 295.4 K according to the recordings.

150 **Table 1.** Summary of the recordings of the Q1-Q4, S0 and S1 (2-0) transitions of H<sub>2</sub>

	<b>Q4</b>	<b>Q3</b>	<b>Q2</b>	<b>Q1</b>	<b>S0</b>	<b>S1</b>
Position (cm <sup>-1</sup> ) [21]	7971.1001	8017.1831	8051.9877	8075.3074	8406.3609	8604.2151
Intensity (cm/molecule) [21]	1.04×10 <sup>-29</sup>	2.36×10 <sup>-28</sup>	3.29×10 <sup>-28</sup>	2.60×10 <sup>-27</sup>	1.56×10 <sup>-27</sup>	5.24×10 <sup>-27</sup>
Pressure (Torr)	Number of recordings					
1				<sup>a</sup>	63	31
5				<sup>a</sup>	50	40
10		34	63	10 <sup>a</sup>	19	11
45		5	7	8	51	40
90	5	6	5	10	16	
210	6	5	7	10	57	
500	7	6	6	8	72	
750	7	7	5	6	36	

151 *Note*  
 152 <sup>a</sup> Additional series of 30 to 100 spectra were recorded for pressures between 2 and 10 Torr, with a  
 153 pressure step of 1 Torr. These spectra (525 in total) were analyzed as an independent dataset.  
 154

155 We recall that the studied H<sub>2</sub> lines are observed superimposed to the broad H<sub>2</sub> collision induced  
 156 absorption (CIA) band which extends from 7800 to 9200 cm<sup>-1</sup> [31], [32]. In the present recordings  
 157 limited to narrow spectral intervals around the H<sub>2</sub> lines, the CIA shows up as an increase of the  
 158 baseline level of the CRDS spectra. Being due to dipole moments induced by interactions between  
 159 colliding H<sub>2</sub> molecules, the CIA has a pressure squared dependence. The sensitivity of the CRDS  
 160 technique and the stability of the setup allow for the measurements of such weak CIA at sub-  
 161 atmospheric pressures. In [20], the  $P^2$  dependence of the baseline level around the Q1 line was  
 162 checked up to 1 atm and the corresponding CIA binary cross-section coefficient was determined. A  
 163 systematic measurements of the H<sub>2</sub> CIA first overtone band in the region accessible with the current  
 164 ECDL (8000-8650 cm<sup>-1</sup>) will be undertaken in the future for validation tests of the semi-empirical CIA  
 165 values [31], [32] largely used for planetary applications.

## 166 **Line parameter retrieval**

167 As mentioned earlier, the standard Voigt profile is not sufficient to adequately model the data  
168 due to the prevalence of narrowing effects in H<sub>2</sub>, justifying the use of more sophisticated line shapes.  
169 The Nelkin-Ghatak profile (NGP) includes the Dicke effect, characterized by the frequency of the  
170 velocity-changing collisions parameter,  $\nu_{VC}$ , in the hard-collision model. The quadratic speed-  
171 dependent Nelkin-Ghatak profile (qSDNGP) further takes into account the speed dependence of the  
172 broadening and shift ( $\gamma_2$  and  $\delta_2$ , respectively), modeled with a quadratic law, leading to a narrowing  
173 and asymmetry of the line profile. As for the self-induced pressure shift and broadening ( $\delta_0$ , and  $\gamma_0$ ,  
174 respectively), the unit of the  $\nu_{VC}$ ,  $\gamma_2$  and  $\delta_2$  parameters is  $\text{cm}^{-1}\text{atm}^{-1}$ . The fitting program MATS [33]  
175 developed at NIST, based on the HAPI Python library and the Levenberg-Marquardt minimizing  
176 algorithm, was used to fit the parameters of the qSDNG profile to the spectra.

177 The recorded spectra were typically  $0.5 \text{ cm}^{-1}$  wide. Some of the lines (S1, S0 and Q1) were  
178 affected by interference from strong water lines in the same spectral region present due to outgassing  
179 (see **Fig. 2**). These water lines were identified on the basis of the recently published [34] line list. In  
180 the case of the S1 line, a H<sub>2</sub><sup>17</sup>O line was situated less than  $0.05 \text{ cm}^{-1}$  from the H<sub>2</sub> line, strongly  
181 affecting the observed position if it was not included in the fit. The observed isotopic abundance of  
182 H<sub>2</sub><sup>17</sup>O and HDO were very different from natural abundance due to previous measurements of  
183 isotopically enriched water in the same CRDS cell, and were determined experimentally by recording  
184 spectra while evacuating the cell. In the analysis, water lines were simulated as Voigt profiles using  
185 line parameters from [34]. The water mole fraction was floated during the analysis of the S1, S0 and  
186 Q1 spectra, and varied between approximately 10 and 200 ppm, well beyond the sub-ppm amount  
187 stated in the gas sample. No water interference was observed for the other Q lines.

188 The analysis was performed in two steps, separately for each line. Firstly, a subset of spectra  
189 (one for each pressure value) was fit in a multi-spectrum configuration to determine the line shape  
190 parameters (broadening, speed dependent parameters for more advanced profiles). The multi-spectrum  
191 fitting procedure constrained the pressure broadening coefficient ( $\gamma_0$ ) and the  $\nu_{VC}$ ,  $\gamma_2$ ,  $\delta_2$  parameters to  
192 be identical for the different pressure values but the positions and line areas were fitted independently  
193 for each spectrum,  $\delta_0$  being fixed to zero. The baseline of each spectrum was adjusted as a linear  
194 function of frequency. **Figure 3** presents such a subset of spectra for the Q1 and Q2 lines, along with  
195 the (meas. - calc.) residuals from the multi-spectrum fits (panel (b)). Note the increase of the baseline  
196 level with increasing pressure due to the CIA contribution. The line shape parameters ( $\gamma_0$ ,  $\nu_{VC}$ ,  $\gamma_2$ ,  $\delta_2$ )  
197 obtained for each line are given in **Table 2**. We have also tried fitting the line shape parameters  
198 separately for each pressure value, fitting all spectra recorded at a given pressure value together. As  
199 can be seen in the lower panel (c) of **Figure 3**, the fit quality is better. Nevertheless, the line  
200 parameters appear to vary in a somewhat non-linear manner with pressure and the speed-dependent  
201 shift parameter  $\delta_2$  could not be determined with good precision at lower pressure values leading to



202 much uncertainty on the apparent line position. For this reason, we chose to use the line shape  
 203 parameters from the constrained fits in the rest of the analysis.

204 **Table 2:** Line shape parameters obtained from multi-spectrum treatment of the CRDS spectra recorded for a  
 205 series of pressure values using a qSDNGP profile. The  $\delta_0$ ,  $\gamma_0$ ,  $\nu_{VC}$ ,  $\gamma_2$ , and  $\delta_2$  values are given in  $10^{-3} \text{ cm}^{-1} \text{ atm}^{-1}$   
 206 unit. For a pressure series, the  $\gamma_0$ ,  $\nu_{VC}$ ,  $\gamma_2$ , and  $\delta_2$  values were constrained to be identical but the line centers and  
 207 line areas were fitted independently for each spectrum, and used afterwards to derive the zero-pressure position  
 208 ( $\nu_0$ ), line intensity ( $S$ ) and self-pressure shift ( $\delta_0$ ). The line intensity was directly converted to the reference  
 209 temperature 296 K in the MATS program. For each line, the line position and shift obtained using the simpler  
 210 NGP profile (with no speed dependence, i.e.  $\gamma_2$  and  $\delta_2$  fixed to zero) are given in italics in the row below. The  
 211 uncertainties given within parenthesis in the unit of the last quoted digit correspond to the ( $1\sigma$ ) statistical values  
 212 provided by the fit. The NGP uncertainty values are identical to the qSDNGP values and not repeated.

213

	$\nu_0$ ( $\text{cm}^{-1}$ )		$S$ (296 K) <sup>c</sup> ( $10^{-28}$ cm/molecule)	$\delta_0$	$\gamma_0$	$\nu_{VC}$	$\gamma_2$	$\delta_2$
	Ab initio <sup>a</sup>	Measured						
<b>Q4</b>	7971.10017(5)	7971.1003373(893) 7971.1003193(893)	0.10534(7)	-2.43(14) -2.95(14)	4.98 3.12	22.38 35.54	7.01	0.77
<b>Q3</b>	8017.18316(5)	8017.1832480(238) 8017.1832481(238)	2.3759(6)	-2.93(24) -3.45(24)	5.85 3.87	21.34 34.89	7.23	0.68
<b>Q2</b>	8051.98773(5)	8051.9878210(114) 8051.9878211(114)	3.2982(4)	-3.10(13) -3.58(13)	5.80 3.45	21.25 33.26	7.07	0.62
<b>Q1</b>	8075.30747(5)	8075.3075828(23) 8075.3075825(23)	26.021(3)	-3.25(2) -3.72(2)	5.18 3.21	20.85 34.25	7.18	0.61
<b>Q1<sup>b</sup></b>		8075.3075822(10) 8075.3075822(10)	25.915(1)	-3.05(4) -4.25(4)	6.66 2.94	12.24 25.27	9.04	1.59
<b>S0</b>	8406.36086(5)	8406.3609484(20) 8406.3609487(20)	15.554(1)	-3.08(1) -3.64(1)	4.90 3.24	21.72 34.51	5.74	0.75
<b>S1</b>	8604.21519(5)	8604.2152759(10) 8604.2152760(10)	52.380(3)	-2.53(3) -3.75(3)	6.16 2.82	10.77 26.01	12.04	1.44

214

215

Notes

216

<sup>a</sup> Ab initio values provided by the H2spectre software [35].

217

<sup>b</sup> Parameters obtained from the separate series of recordings between 2 and 10 Torr (see Table 1 and  
 218 experiment section).

219

<sup>c</sup> The given intensity values include the H<sub>2</sub> isotopic abundance factor (0.9997)

220

221

222

223

224

225

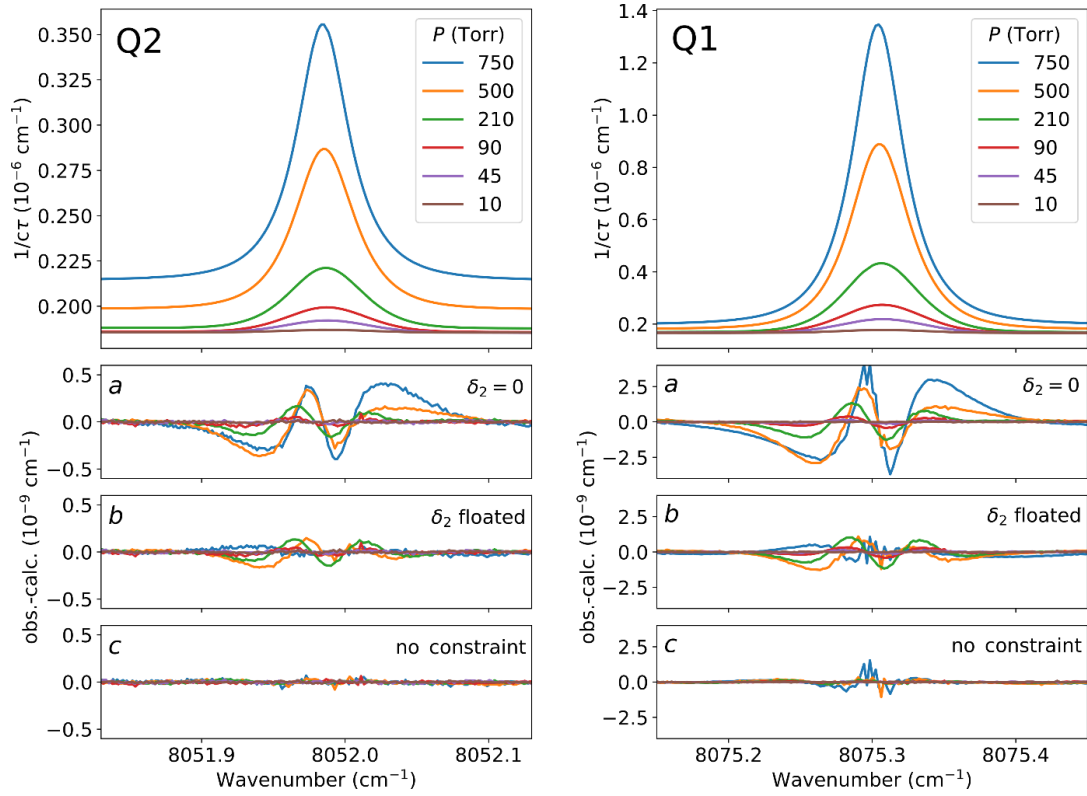
226

227

228

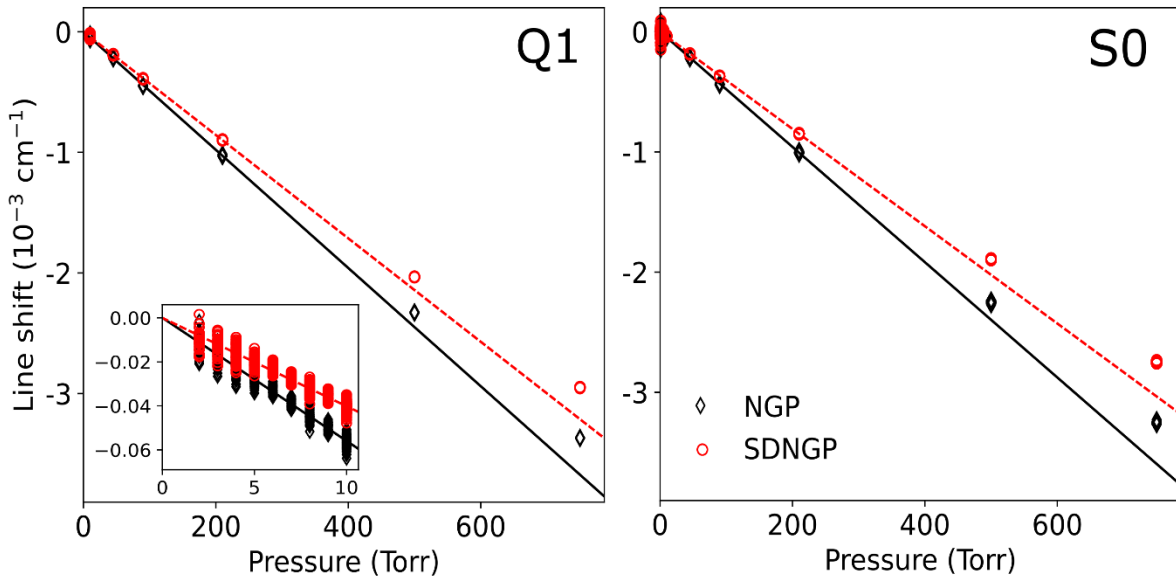
229

In a second step, all spectra were fit separately, fixing the line shape parameters to the values  
 determined in the first step, and floating only the position and intensity. **Figure 4** presents the apparent  
 line positions as a function of pressure, for lines Q1 and S0. The zero-pressure line position and the  
 pressure shift coefficient were obtained from a linear regression of the apparent line centers vs.  
 pressure. As a clear departure from the linearity is observed at high pressure (see **Fig. 4**), the linear  
 regression was performed only below 210 Torr. In the case of the Q1 line, we have included an inset  
 corresponding to the separate series of recordings between 2 and 10 Torr. An excellent agreement  
 (better than 20 kHz) is achieved between the two independent determinations of the zero-pressure Q1  
 line positions.



230

231 **Fig. 3** Sample of spectra of the Q2 (left) and Q1 (right) lines, recorded at various pressures and used to  
 232 determine the line shape parameters. The panels present the experimental spectra (top), and the residuals of a  
 233 multi-spectrum fit with qSDNGP profile and three different configurations: with all parameters constrained and  
 234 (a)  $\delta_2$  fixed to zero, or (b)  $\delta_2$  floated; (c) with all parameters determined separately for each pressure. Note the  
 235 different vertical scale for the two lines, and the increase in the baseline at higher pressure due to CIA.



236

237 **Fig. 4** Determination of the zero-pressure position from a linear extrapolation of the apparent qSDNGP and  
 238 NGP line positions, for the lines Q1 and S0. The linear regression was performed below 210 Torr due to the  
 239 clear non-linearity of the observed shift at higher pressures. This plot also illustrates the difference in apparent  
 240 position due to the inclusion of the speed-dependence of the pressure shift ( $\delta_2$ ) which takes into account the  
 241 asymmetry of the line profile (see the residuals in Fig. 3). The insert on the Q1 panel corresponds to the separate  
 242 series of recordings between 2 and 10 Torr (see Text).  
 243

244 In order to evaluate the impact of the choice of the profile to the zero-pressure positions, we  
245 also applied the procedure described above using simpler line profiles: NGP which does not include  
246 the speed dependence of the broadening and shift ( $\gamma_2=0$  and  $\delta_2=0$ ), and qSDNGP with  $\delta_2$  fixed to  
247 zero. The positions obtained with these two simpler profiles are very close but differ importantly from  
248 the qSDNGP positions (see **Fig. 4**). This observation evidences the importance of the speed-  
249 dependence of the collisional shift ( $\delta_2$ ) on the apparent line position at a given pressure value. This is  
250 reflected by the larger residuals obtained with  $\delta_2=0$  (**Fig. 3a**). Nevertheless, as illustrated in **Fig. 4**, the  
251 zero-pressure position is found mostly identical for the different profiles (within a few kHz). The  
252 position and line shift values obtained using a NGP profile are included in **Table 2**. Let us mention  
253 that the NGP pressure shift parameters of the Q1-Q4 lines agree with the values retrieved in [17] using  
254 a Galatry profile (both NGP and Galatry profiles neglect speed dependent effects).

255 From **Table 2**, it appears that all the values of the profile parameters of the different lines are  
256 consistent except those relative to the separate series of Q1 recordings with maximum pressure of 10  
257 Torr and those of the S1 recordings with maximum pressure of 45 Torr. This observation indicates that  
258 the line parameters depend not only on the chosen profile but also on the maximum pressure of the  
259 recordings used for their determination. The reader is referred to [25] and [26] for a detailed  
260 discussion of the correlation between the profile parameters and an improved treatment of the Q1 (2-0)  
261 and Q1 (3-0) profiles using a corrected Hartmann-Tran profile adjusted to particular model of the  
262 velocity-changing collisions.

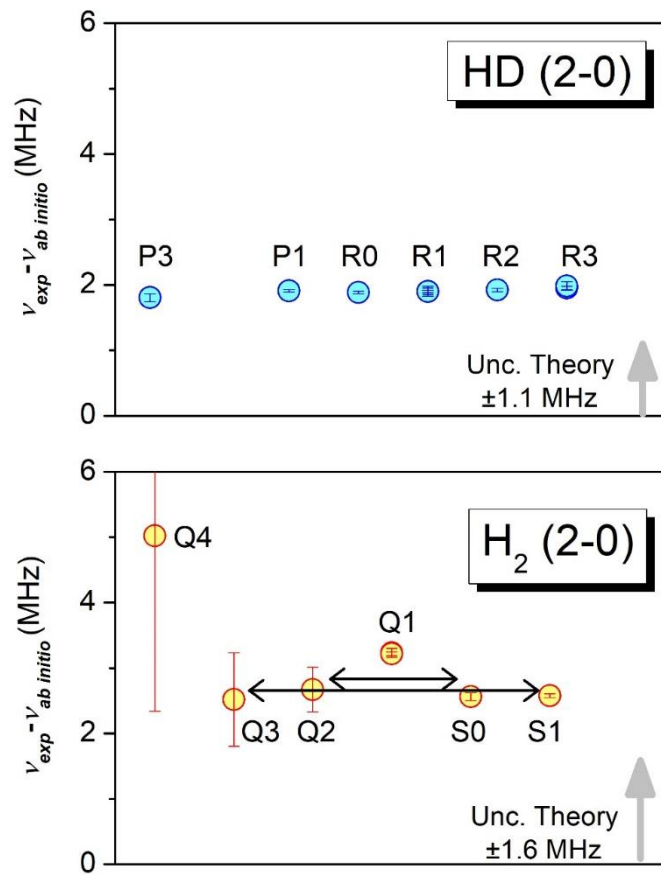
263 Line intensities were floated for each spectrum and obtained as the average of the line intensity  
264 values weighted by their fit uncertainty. The agreement between the reported intensities (**Table 2**) and  
265 HITRAN values (**Table 1**) is excellent: the four determinations of the Q1, S0 and S1 line intensities  
266 lead to an average intensity ratio of 1.0013 with a standard deviation less than 0.0020. The largest  
267 relative deviation for the very weak Q4 line with intensity of  $1.04 \times 10^{-29}$  cm/molecule is less than 1%.  
268 This level of agreement validates with an unprecedented accuracy the *ab initio* intensity values of [37]  
269 reproduced in the HITRAN database [21]. We note that the uncertainty of 10% attached to the  
270 HITRAN intensity value is largely overestimated.

### 271 **Comparison with *ab initio* calculations**

272 In the recent years, significant progress has been achieved in the *ab initio* calculations of the H<sub>2</sub>,  
273 HD and D<sub>2</sub> energy levels [1], [2], [3], [36]. In these works, the authors performed 4-particle fully  
274 variational calculations including relativistic and quantum electrodynamics (QED) effects in the  
275 nonadiabatic treatment of the nuclear motion. The resulting calculated transition frequencies of the six  
276 H<sub>2</sub> transitions presently studied, as provided by the H2spectre software [35], are included in **Table 2**.  
277 The corresponding deviations from the experimental values are displayed on the lower panel of **Fig. 5**.

278 The first observation is that the deviations obtained for Q3, Q2, S0 and S1 are very close, with  
279 an average value of 2.58 MHz and a standard deviation of only 63 kHz. The Q1 transition frequency

280 determined shows a higher deviation of 3.23 MHz and appears to be an outlier. For comparison  
 281 purpose, we present on the upper panel of **Fig. 5**, a similar plot for the six (electric dipole) transitions  
 282 of HD in the (2-0) band whose transition frequencies have been recently measured at high accuracy.  
 283 The experimental values obtained in saturation regime [8], [10], [11] and in Doppler regime [16], [17]  
 284 have a similar accuracy of a few tens of kHz. Very similar (meas.-calc.) frequency differences are  
 285 obtained for the six HD transitions which are on average 1.91 MHz larger than predicted by theory  
 286 with a standard deviation of only 49 kHz. Let us note that for both H<sub>2</sub> and HD, the calculated  
 287 frequencies are underestimated and deviate on average by about 1.7 times their claimed uncertainties  
 288 (1.6 and 1.1 MHz, respectively). The absence of rotational dependence of the deviations leads to the  
 289 conclusion that the V=2 vibrational term is underestimated by theory, both for H<sub>2</sub> and HD.



290  
 291 **Fig. 5** Differences between experiment and theory for the most accurate experimental frequency determinations  
 292 in the first overtone band of HD and H<sub>2</sub> (upper and lower panels, respectively). The theoretical values  
 293 [Puchalski2019] were obtained from the H2spectre software [35]. The grey arrows represent the uncertainty on  
 294 the calculated values (1.1 and 1.6 MHz, respectively). The H<sub>2</sub> experimental values are obtained in the present  
 295 work while the HD experimental values were reported in [8], [10], [11], [16], [17]. The black arrows on the  
 296 lower panel connect pairs of transitions involved in ground state combination relations.  
 297

298 While the uncertainties on the *ab initio* transition frequencies are much larger than the  
 299 corresponding experimental error bars (about one MHz compared to few tens of kHz), the energy  
 300 separations between the ground state rotational levels are predicted with a much better accuracy,

301 allowing for more stringent validation tests. The lower uncertainty on the energy separation is  
 302 probably related to error cancellations in the computation of the energy levels.

303 Combination differences of measured transition frequencies can be used to derive accurate  
 304 values of the energy level separation in the ground vibrational state. From the six presently measured  
 305 H<sub>2</sub> (2-0) transition frequencies, the energy separation between the  $J= 2$  and  $J= 0$  levels,  $\Delta_{(J= 2)-(J= 0)}$  is  
 306 obtained by difference of S0 and Q2 transition frequencies sharing the same  $J= 2$  ( $V=2$ ) upper level.  
 307 Similarly, the separation between the  $J= 3$  and  $J= 1$  levels,  $\Delta_{(J= 3)-(J= 1)}$ , is obtained by difference of S1  
 308 and Q3 transition frequencies. The comparison summarized in **Table 3** shows a convincing agreement  
 309 between theory and experiment, within 100 kHz for both  $\Delta_{(J= 2)-(J= 0)}$  and  $\Delta_{(J= 3)-(J= 1)}$ . This level of  
 310 agreement is surprisingly good as it is better than the uncertainties on the *ab initio* values (110 and 180  
 311 kHz, respectively) which are themselves significantly better than the uncertainties on the experimental  
 312 values (390 and 750 kHz, respectively).

313 In summary, the experimental data at disposal confirm the sub-MHz accuracy of the energy  
 314 separation of the *ab initio* ground state energy levels and seem to indicate that the 1.6 MHz claimed  
 315 uncertainty on the *ab initio* frequencies of the studied (2-0) transitions is underestimated.

316  
 317 **Table 3.** Energy separations between ground state rotational levels obtained by combination differences  
 318 of the measured and calculated transitions. The difference between the  $J= 2$  and  $J= 0$  energy levels is obtained  
 319 from the S0 and Q2 transition frequencies. That between the  $J= 3$  and  $J= 1$  energy levels is obtained from the S1  
 320 and Q3 transition frequencies. The ( $1\sigma$ ) uncertainties are given within parenthesis in the unit of the last quoted  
 321 digit.

322

	Exp. (MHz)	Calc. (MHz)	Exp. (cm <sup>-1</sup> )	Calc. (cm <sup>-1</sup> )
$\Delta_{(J= 2)-(J= 0)}$	10 623 839.09(39)	10 623 839.17(11)	354.373 127(13)	354.373 130(4)
$\Delta_{(J= 3)-(J= 1)}$	17 598 777.46(75)	17 598 777.37(18)	587.032 028(25)	587.032 025(6)

323

324 Compared to the average value for the Q3, Q2, S0 and S1 positions, the 650 kHz offset of the  
 325 Q1 frequency difference to theory remains to be explained. We considered a possible experimental  
 326 bias due to an underlying impurity line located in the range of the Q1 line profile but the typical  
 327 concentration of water vapor in our spectra leads to a negligible contribution of this species. A  
 328 systematic search of the possible absorbers on the basis of the HITRAN database indicates that a weak  
 329 ammonia line could be present in the range of the Q1 profile but the spectra do not show stronger  
 330 ammonia lines located in the vicinity. Let us recall, that the Q1 transition frequency reported in this  
 331 work was retrieved from spectra recorded in two measurement campaigns, three years apart and an  
 332 agreement within 18 kHz is obtained between the two determinations. Thus the origin of the 650 kHz  
 333 offset of the Q1 frequency is unexplained so far. As the O3 (2-0) transition at 7488.27 cm<sup>-1</sup> is sharing  
 334 the same  $J= 1$  ( $V=2$ ) upper level than the Q1 transition, the (planned) accurate measurement of the O3

335 transition frequency should bring a decisive confirmation on the existence and on the amplitude of this  
336 offset.

337 In summary, the transition frequencies reported in the present work are the most accurate  
338 reported so far for H<sub>2</sub>, the first ones in the (2-0) band referenced to an absolute frequency standard.  
339 Their relative uncertainty is at the 10<sup>-10</sup> level in the case of the Q1, S0 and S1 transitions. The  
340 comparison to the most recent theoretical values shows a systematic underestimation of 2.58 MHz of  
341 the calculated transition frequencies, a situation similar to that found for (2-0) transitions in HD. This  
342 observation provides a challenge for future refinement of the *ab initio* calculations of the energy levels  
343 of the hydrogen molecule. Finally, we note that *ab initio* values of the intensity of the six studied  
344 transitions are validated within a few thousandths.

#### 345 *Conflicts of interest*

346 There are no conflicts to declare.

347

#### 348 *Acknowledgements*

349 AOK acknowledges the support by the French National Research Agency in the framework of the  
350 "Investissements d'avenir" program (ANR-15-IDEX-02). The supports by the REFIMEVE  
351 consortium (Equipex REFIMEVE+ ANR-11-EQPX-0039) and by CNRS (France) in the frame of the  
352 International Research Project SAMIA are acknowledged. AOK acknowledges partial support from  
353 Russian State project No 0030-2021-0016. Communications with K. Pachucki (Warsaw), J. Komasa  
354 (Poznan), W. Ubachs (Amsterdam) and ML. Diouf (Amsterdam) about the *ab initio* values of the H<sub>2</sub>  
355 transition frequencies are acknowledged.

356  
357  
358  
359  
360  
361  
362  
363  
364  
365  
366  
367  
368  
369  
370  
371  
372  
373  
374  
375  
376  
377  
378  
379  
380  
381  
382  
383  
384  
385  
386  
387  
388  
389  
390  
391  
392  
393  
394  
395  
396  
397  
398  
399  
400  
401  
402  
403  
404  
405

References

1. P. Czachorowski, M. Puchalski, J. Komasa and K. Pachucki, *Phys. Rev. A*, 2018, **98**, 052506.
2. M. Puchalski, A. Spyszkiwicz, J. Komasa and K. Pachucki, *Phys. Rev. Lett.*, 2018, **121**, 073001.
3. M. Puchalski, J. Komasa, A. Spyszkiwicz and K. Pachucki, *Phys. Rev. A*, 2019, **100**, 020503.
4. H. Józwiak, H. Cybulski and P. Wcisło, *J. Quant. Spectrosc. Radiat. Transf.*, 2020, **256**, 107255.
5. M. Puchalski, J. Komasa and K. Pachucki, *Phys. Rev. Lett.*, 2020, **125**, 253001.
6. P. Dupré, *Phys. Rev. A*, 2020, **101**, 022504.
7. A. Campargue, S. Kassı, K. Pachucki and J. Komasa, *Phys. Chem. Chem. Phys.*, 2012, **14**, 802.
8. F. M. J. Cozijn, P. Dupré, E. J. Salumbides, K. S. E. Eikema and W. Ubachs, *Phys. Rev. Lett.*, 2018, **120**, 153002.
9. F. M. J. Cozijn, M. L. Diouf, V. Hermann, E. J. Salumbides, M. Schlösser and W. Ubachs, *Phys. Rev. A*, 2022, **105**, 062823.
10. M. L. Diouf, F. M. J. Cozijn, B. Darquié, E. J. Salumbides and W. Ubachs, *Opt. Lett.*, 2019, **44**, 4733.
11. M. L. Diouf, F. M. J. Cozijn, K.-F. Lai, E. J. Salumbides, and W. Ubachs, *Phys. Rev. Research*, 2020, **2**, 023209.
12. T.-P. Hua, Y. R. Sun and S.-M. Hu, *Opt. Lett.*, 2020, **45**, 4863.
13. A. Fast and S. A. Meek, *Phys. Rev. Lett.*, 2020, **125**, 023001.
14. M. L. Niu, E. J. Salumbides, G. D. Dickenson, K. S. E. Eikema and W. Ubachs, *J. Mol. Spectr.*, 2014, **300**, 44.
15. A. Castrillo, E. Fasci and L. Gianfrani, *Phys. Rev. A*, 2021, **103**, 022828.
16. A. Castrillo, E. Fasci and L. Gianfrani, *Phys. Rev. A*, 2021, **103**, 069902.
17. S. Kassı, C. Lauzin, J. Chaillot and A. Campargue, *Phys. Chem. Chem. Phys.*, 2022, **24**, 23164.
18. C.-F. Cheng, Y.R. Sun, H. Pan, J. Wang, A.W. Liu, A. Campargue, S.-M. Hu, *Phys. Rev. A*, 2012, **85**, 024501.
19. S. -M. Hu, H. Pan, C.-F Cheng, X.-F. Li, J. Wang, A. Campargue and A.W. Liu, *Astrophys. J.*, 2012, **749** (1), 76.
20. S. Kassı, A. Campargue, *J. Mol. Spectrosc.*, 2014, **300**, 55.
21. I.E. Gordon, L.S. Rothman, R.J. Hargreaves, R. Hashemi, E.V. Karlovets et al., *J. Quant. Spectrosc. Radiat. Transf.*, 2021, **277**, 107949.
22. S. L. Bragg, J. W. Brault and W. H. Smith, *Astrophys. J.*, 1982, **263**, 999.
23. P. Wcisło, H. Tran, S. Kassı, A. Campargue, F. Thibault and R. Ciurylo. *J. Chem. Phys.*, 2014, **141**, 074301.
24. P. Wcisło, I.E. Gordon, H. Tran, Y. Tan, S.-M. Hu, A. Campargue, S. Kassı, D. Romanini, C. Hill, R.V. Kochanov and L.S. Rothman, *J. Quant. Spectrosc. Radiat. Transf.*, 2016, **177**, 75.
25. D. Mondelain, T. Sala, S. Kassı, D. Romanini, M. Marangoni and A. Campargue, *J. Quant. Spectrosc. Radiat. Transf.*, 2015, **154**, 35.
26. D. Mondelain, S. Kassı, T. Sala, D. Romanini, M. Marangoni and A. Campargue, *J. Mol. Spectrosc.*, 2016, **326**, 5.
27. M. Konefał, S. Kassı, D. Mondelain, A. Campargue, *J. Quant. Spectrosc. Radiat. Transf.*, 2020, **241**, 106653.
28. S. Vasilchenko, H. Tran, D. Mondelain, S. Kassı, A. Campargue, *J. Quant. Spectrosc. Radiat. Transf.*, 2019, **235**, 332.
29. B. Bordet, S. Kassı, A. Campargue, *J. Quant. Spectrosc. Radiat. Transfer*, 2021, **260**, 107453.
30. D. Mondelain, S. Vasilchenko, S. Kassı, A. Campargue. *J. Quant. Spectrosc. Radiat. Transf.*, 2020, **253**, 107020.
31. W. Meyer, A. Borysow, L. Frommhold, *Phys. Rev. A*, 1993, **47**, 4065.
32. M. Abel, L. Frommhold, X. Li, K.L.C. Hunt, *J. Phys. Chem. A*, 2011, **115** (25), 6805.
33. E.M. Adkins, MATS: Multi-spectrum Analysis Tool for Spectroscopy, 2020.
34. A.O. Koroleva, S.N. Mikhailenko, S. Kassı, A. Campargue, *J. Quant. Spectrosc. Radiat. Transf.*, 2023, **298**, 108489.

- 406 35. P. Czachorowski, H2SPECTRE version 7.3, Fortran source code, 2020, Ph.D. thesis, University of  
407 Warsaw, 2019, <https://www.fuw.edu.pl/~krp/codes.html>;  
408 <http://qcg.home.amu.edu.pl/H2Spectre.html>.  
409 36. J. Komasa, K. Piszczatowski, G. Łach, M. Przybytek, B. Jeziorski and K. Pachucki, *J. Chem. Theory*  
410 *Comput.*, 2011, **7** (10), 3105.  
411 37. L. Wolniewicz, I. Simbotin, A. Dalgarno, *Astrophys. J., Suppl. Ser.*, 1998, **115**, 293.